Analytical Methods

Rapid electrotransfer probing for improved detection sensitivity in in-gel immunoassays

Journal:	*Analytical Methods*
Manuscript ID	AY-ART-06-2020-001203.R1
Article Type:	Paper
Date Submitted by the Author:	14-Aug-2020
Complete List of Authors:	Mourdoukoutas, Andoni; UC Berkeley and UC San Francisco Graduate Program in Bioengineering, Grist, Samantha; University of California Berkeley, Department of Bioengineering Herr, Amy; University of California, Berkeley, Department of Bioengineering; Chan Zuckerberg Biohub

PAPER

Rapid electrotransfer probing for improved detection sensitivity in in-gel immunoassays

Andoni P Mourdoukoutas,[a] Samantha M Grist[b] and Amy E Herr[a,b,c,*]

6565Received 00th January 20xx,
Accepted 00th January 20xx

DOI: 10.1039/x0xx00000x

Protein electrotransfer in conventional western blotting facilitates detection of size-separated proteins by diffusive immunoprobing, as analytes are transferred from a small-pore sizing gel to a blotting membrane for detection. This additional transfer step can, however, impair detection sensitivity through protein losses and confound protein localization. To overcome challenges associated with protein transfer, in-gel immunoassays immobilize target proteins to the hydrogel matrix for subsequent in-gel immunoprobing. Yet, detection sensitivity in diffusive immunoprobing of hydrogels is determined by the gel pore size relative to the probe size, and in-gel immunoprobing results in (i) reduced in-gel probe concentration compared to surrounding free-solution, and (ii) slow in-gel probe transfer compared to immunocomplex dissociation. Here, we demonstrate electrotransfer probing for effective and rapid immunoprobing of in-gel immunoassays. Critically, probe (rather than target protein) is electrotransferred from an inert, large-pore 'loading gel' to a small-pore protein sizing gel. Electric field is used as a tuneable parameter for electromigration velocity, providing electrotransfer probing with a fundamental advantage over diffusive probing. Using electrotransfer probing, we observe 6.5 ± 0.1 X greater probe concentration loaded in-gel in ~82X time reduction, and 2.7 ± 0.4 X less probe concentration remaining in-gel after unloading in ~180X time reduction (compared to diffusive probing). We then apply electrotransfer probing to detect OVA immobilized in-gel and achieve 4.1 ± 3.4 X greater signal-to-noise ratio and 30X reduction in total immunoprobing duration compared to diffusive probing. We demonstrate electrotransfer probing as a substantially faster immunoprobing method for improved detection sensitivity of protein sizing in-gel immunoassays.

Introduction

Proteins are key drivers of a range of biological processes,[1] and protein quantification from biological samples is an important metric for understanding cell and tissue state.[2] Protein detection can be accomplished by in-gel immunoassays, in which proteins are immobilized to a hydrogel matrix for subsequent immunoprobing. In-gel protein immobilization can also provide structural integrity to a biological sample, assess protein localization, and perform protein sizing.[3,4,5,6,7] Probing in-gel immunoassays involves (i) probe loading into the immunoassay gel, (ii) in-gel probe incubation for equilibrium immunocomplex formation, and (iii) unloading of unbound probe from the immunoassay gel (Figure 1A-C).[8] The concentration of immunocomplex remaining at time of assay readout is dependent on the concentration of probe loaded in-gel ($[Ab]_{gel}$; mol·m^{-3}) and the immunocomplex dissociation during unbound probe unloading. In a bimolecular system, the equilibrium immunocomplex formation ($[AbAg]_{max}$; mol·m^{-3}) in step (ii) is dependent on $[Ab]_{gel}$ by[9]

$$\frac{[AbAg]_{max}}{[Ag]_{gel}} = \frac{1}{1 + \frac{K_D}{[Ab]_{gel}}} \quad (1)$$

where $[Ag]_{gel}$ is the target protein concentration, and K_D (m^3·mol^{-1}) is the equilibrium dissociation constant (Figure 1D). In the absence of new binding events, $[AbAg]_{max}$ dissociates during step (iii) according to the dissociation rate constant (k_{off}; s^{-1})[9]

$$\frac{[AbAg]_t}{[AbAg]_{max}} = 1 - exp(-k_{off}t) \quad (2)$$

where $[AbAg]_t$ (mol·m^{-3}) is the immunocomplex remaining at time t (s) (Figure 1E).

In diffusive probe loading from free-solution to a hydrogel, the in-gel probe concentration is highly dependent on the gel pore size compared to the probe size.[10,11] Small pores relative to the size of the probe impedes diffusive probe loading to a hydrogel. At equilibrium, diffusively loaded $[Ab]_{gel}$ is less than the free-solution probe concentration ($[Ab]_{sol}$) due to size-exclusion partitioning. The ratio of $[Ab]_{gel}$ to $[Ab]_{sol}$ at equilibrium is the probe partition coefficient (K_{part}). In hydrogels that use small gel pores (10-100 nm) to separate proteins by size, K_{part} < 0.2 has been observed[3,12] for large antibody probes (hydrodynamic radius ~5 nm)[13] diffusively loaded into the hydrogel.

To decouple the gel pore size demands for protein sizing from the gel requirements for effective probe loading (K_{part}~1), target proteins

[a] The UC Berkeley/UCSF Graduate Program in Bioengineering, University of California Berkeley, Berkeley, California 94720, United States
[b] Department of Bioengineering, University of California Berkeley, Berkeley, California 94720, United States
[c] Chan Zuckerberg Biohub, San Francisco, California 94158, United States
* Corresponding author
Electronic Supplementary Information (ESI) available: [details of any supplementary information available should be included here]. See DOI: 10.1039/x0xx00000x

in western blotting are electrotransfered from a small-pore protein sizing gel to a large-pore blotting membrane (e.g. nitrocellulose or PVDF, 200-450 nm pores).[14,15,16,17,18] However, while performing protein sizing and immunoprobing in separate materials allows for pore sizes to be independantly optimized for each step, target protein can be lost from the assay by incomplete gel-membrane electrotransfer (total protein mass captured by membrane less than protein mass in gel).[14] The extent of protein mass loss in gel-membrane electrotransfer is also target specific, complicating analyte quantification.[14] Additionally, protein sizing separation resolution is reduced by diffusive broadening of separated protein bands during electrotransfer.[14,17] By minimizing protein diffusive broadening and loss timescales, protein size characterizations from single-cells have been performed using in-gel protein immobilization.[3] In-gel protein immobilization has also made possible 3-D protein localization in tissue through hydrogel-tissue hybrid immunoassays.[4,5]

To preserve advantages of performing immunoassays in-gel, a class of diffusive probe loading techniques increases equilibrium in-gel probe concentration, and thus K_{part}, by leveraging electrostatic interactions between charged molecules and charged hydrogels,[19] dehydrating in-gel immunoassays prior to probe loading,[8] and forming bi-phasic systems using salts and PEG.[20] While importantly biasing the probe partitioning equilibrium towards the hydrogel, these methods do not expedite unloading of unbound probe. The time over which immunocomplex dissociates during probe unloading thus remains unchanged.

Electrophoretic probing has been demonstrated in microcapillary gel systems as a method for both overcoming size-exclusion partitioning and rapidly loading and unloading probe compared to diffusive probe transfer.[21,22] These important demonstrations of electrophoretic probing have been shown to improve immunoassay sensitivity, including in small-pore, protein sizing in-gel immunoassays.[21] However, the applicable assay designs have been confined to enclosed microchannels and capillaries, increasing complexity of assay design, limiting sample throughput, and requiring unique microchip probe reservoir design for each microchannel immunoassay. In contrast to encapsulated microchannels, 'open' microfluidic systems remove contraints to biological samples and pre-processing steps by eliminating at least one confining boundary of the fluid sample.[23,24,25] Sample fluid accessibility is also facilitated in open devices by featuring at least one liquid-liquid or liquid-vapor interface. A generalized electrophoretic probing system that can be widely applied to millimeter-scale, open planar format in-gel protein sizing immunoassays[7] has not yet been demonstrated.

Here, we introduce a generalized electrotransfer probing platform for improved detection sensitivity of open, millimeter-scale, small-pore protein sizing in-gel immunoassays compared to diffusive probing. The platform builds on principles of gel-membrane electrotransfer used in conventional western blotting, but critically electrotransfers probe (instead of target protein) from an inert, large-pore gel to an in-gel immunoassay. We evaluated our design in comparison to diffusive probing by investigating maximum probe loading and unloading, and timescales for achieving maximum probe loading and unloading in a protein sizing gel. Finally, we demonstrate electrotransfer probing for significantly improved in-gel immunoassay signal-to-noise ratio (SNR) in substantially less time (compared to diffusive probing) by using detection of OVA immobilized in a protein sizing gel as a model system.

Experimental section

Polyacrylamide gel fabrication

Polyacrylamide (PA) gel was used as the molecular sieving matrix, the 20%T PA gels (used in the probe electrophoretic mobility characterization experiments), and the 4%T PA loading gel. The sizing gels were fabricated in moulds that consisted of a glass slide (VWR), a silicon wafer with SU-8 3050 (Microchem) photolithographically-micropatterned features, and two 1 mm thick shims (C.B.S. Scientific Gel Wrap). The glass slide and silicon wafer were separated by the 1 mm thick shims. To pattern a face of the sizing gel with microwell features, SU-8 features were patterned on the silicon wafer by photolithography as previously described.[26] SU-8 features were cylindrical microposts 40 µm in height, 32 µm in diameter and spaced 100 µm apart (center-center feature spacing). To mitigate gel adhesion, the SU-8 layer was coated with dichlorodimethylsilane (No. 440272, Sigma-Aldrich) and the glass slide was treated with Gel Slick® (No. 50640, Lonza). The 20%T PA gels were fabricated between a glass slide and a glass plate (McCormick). The 20%T PA gels and the 4%T PA loading gels were fabricated in moulds that consisted of a glass slide, a glass plate (McCormick), and two 1 mm thick shims. The glass slide and glass plate were separated by the 1 mm thick shims. The glass slide and glass plate were both treated with Gel Slick®. No features were patterned on the 20%T PA gels or 4%T PA loading gels.

Fabrication conditions for PA gels are described in Table S1. The sizing gels were co-polymerized with N-[3-[(3-Benzoylphenyl)-formamido]propyl] methacrylamide (BPMA) to immobilize protein in-gel.[3,26] BPMA can immobilize proteins to the gel matrix by covalently binding to proteins in-gel upon exposure to ultraviolet light.[27] All PA gels were chemically polymerized for 60 min using ammonium persulfate (APS; No. A36778, Sigma-Aldrich) and TEMED (No. T9281, Sigma-Aldrich). PA gel precursor solutions were degassed and sonicated for 5 min before chemical initiators were added. To cast the sizing gel to the fabrication mould, first, the 1 mm thick shims were affixed with adhesive tape to the SU-8 coated silicon wafer. Then, the PA precursor solution was then pipetted onto the SU-8 mould in the gap between the shims (Figure S1A). Next, a glass slide was placed on top of the shims to mould the PA gel precursor solution between the glass slide, the SU-8 coated silicon wafer, and the shims (Figure S1B). After the PA gel polymerized (60 min), the gels were released from the fabrication moulds by sliding a razor between the glass slide and the silicon wafer (in sizing gel fabrication) or the glass plate (in 20%T PA gel and 4%T PA loading gel fabrication) (Figure S1C) and used as a lever to lift the glass slide from the mould. Finally, the 1 mm thick

polymerized PA gels were then trimmed with a razor to the dimensions described in Table S1 (Figure S1D). PA gels were equilibrated in Electrotransfer Buffer (Table S2) at 4 °C for at least 12 h and up to 4 days prior to use.

Probe loading gel fabrication

The loading gel was cast from a mixture of molten 1.5% w/v Ultrapure Low Melting Point Agarose (No. 16520050, Invitrogen) dissolved in 1X Tris-glycine (No. 1610734, Bio-Rad) and fluorescently-labelled antibody (Ab) probe. The sizing gels were fabricated in moulds that consisted of a glass slide, a glass plate, and two 1 mm-thick shims. The glass slide and glass plate were separated by the 1 mm-thick shims.

Fabrication conditions for the loading gels are described in Table S3. To cast the loading gel to the fabrication mould, first, the fabrication mould was assembled: (i) the 1 mm thick shims were affixed with adhesive tape to the glass plate, (ii) the glass slide was affixed with adhesive tape on top of the shims, and (iii) the glass plate was placed on a hotplate and heated to ~35-40 °C (Figure S2A). Temperature measurements were performed by infrared thermometry. Then, the molten mixture of 1.5% w/v agarose and probe was prepared: (i) probe solution was added to a 1.5 mL Eppendorf tube that was warmed to ~35-40 °C on a hot plate (Figure S2B), and (ii) ~40-50 °C molten agarose was added to the antibody probe solution and mixed by pipetting (Figure S2C). Temperatures were optimized to maintain molten state of agarose without exceeding maximum temperature of the probe thermal stability range. Ultrapure Low Melting Point Agarose remains fluid at 37 °C and sets rapidly below 25 °C. IgG antibodies exhibit conformational stability at temperatures <55 °C.[28] Next, the loading gel was cast by pipetting the molten mixture of agarose gel and probe into the fabrication mould (Figure S2D). After casting the loading gel, the loading gel was cooled to gelate by transferring the fabrication mould to an ice pack (Figure S2E). After gelation, the fabrication mould was transferred to a flat surface at ~20 °C, and the loading gel was released from the fabrication mould and trimmed by the same process used for PA gel release and trimming (Figure S2F,G). Finally, the loading gels were dipped in Electrotransfer Buffer and used immediately.

Gel sandwich assembly for electrotransfer probing

To load probe by electrotransfer to a sizing gel, a gel-gel sandwich was made using the loading gel, the sizing gel, two western blot filter paper pieces (1mm thick; No. 84783, Thermo Fisher Scientific), a custom-fabricated acrylic clamp and plastic elastomers. The clamp fabrication is described below in the subsection *Acrylic clamp fabrication.* The filter paper pieces were cut to 55 mm width x 85 mm height to match the clamp dimensions and equilibrated in Electrotransfer Buffer for 5 min prior to assembling the sandwich.

To assemble the gel-gel sandwich used in probe loading, first, the sizing gel was placed on a filter paper piece (Figure S3A). Then, the loading gel was placed on top of the sizing gel without trapping air bubbles in the fluid layer between the gels (gel x-y faces in contact; Figure S3B). Next, the second filter paper piece was placed on top of the loading gel (the edges of the two filter paper pieces were aligned when placing the second filter paper; Figure S3C). The filter paper - gels - filter paper stack was then transferred into the acrylic clamp (Figure S4), and the assembly was compressed together using polymer elastic bands (Scünci Polybands).

To unload probe by electrotransfer from a sizing gel, the same sandwich assembly process that was performed for probe loading was followed, but with the omission of the loading gel. Thus, the sizing gel was placed on a filter paper piece, and the second filter paper piece was placed on top of the sizing gel. The filter paper - sizing gel - filter paper assembly was transferred into the clamp and compressed using plastic elastomers.

Acrylic clamp fabrication

To compress the gel sandwiches used for electrotransfer probing, and suspend the gel sandwiches in the buffer chamber of a slab-gel electrotransfer system, an acrylic clamp was designed and fabricated. Individual clamp components were designed in Adobe® Illustrator® and cut from acrylic sheets (3.175 mm thick acrylic sheets, clear; No. FJ-63961240, Astari) using a laser cutter (laser cutter printing software: RetinaEngrave3D; laser cutter: No. HL40-5G-110, Full Spectrum Laser). The individual components of the clamp were affixed together with super glue. The assembled clamp consisted of two identical halves that were compressed together with plastic elastomers (Figure S4A,B). The clamp was designed to position up to 6 gel sandwiches in the centre of the buffer chamber of a slab-gel electrotransfer system by hanging (and self-aligning) from the top edge of the chamber (XCell SureLock™ Mini-Cell Electrophoresis System, No. EI0001, Invitrogen; XCell II™ Blot Module, No. EI0002, Invitrogen; Figure S4C).

Probe electrotransfer conditions

To perform electrotransfer probe loading or unloading, a gel sandwich was assembled (described in subsection *Gel sandwich assembly for electrotransfer probing*), affixed with the clamp, and suspended in the buffer chamber of the slab-gel electrotransfer system. In electrotransfer probe loading, the loading gel was positioned towards the cathode (-) and the sizing gel was positioned near the anode (+) so that the negatively-charged probe molecules migrated into and through the sizing gel when the field was applied. The buffer chamber was filled with Electrotransfer Buffer, and the outer chamber was filled with ice water (Figure S4C). The entire slab-gel electrotransfer system was placed on ice. The slab-gel electrotransfer system was connected to a power supply (PowerPac High-Voltage Power Supply; No. 1645056, Bio-Rad). The power supply was set to constant voltage, and an electric field was applied. The applied electric field strength and time are described in Table S4. At the completion of electrotransfer probe loading or unloading, the power supply was turned off and the clamp was removed from the slab-gel electrotransfer

system. The polymer elastics were removed from the clamp, and the gels were retrieved. The filter papers were disposed after every use, while the acrylic clamp and polymer elastic bands were rinsed in water and dried before reuse.

Semi-dry electrotransfer system

An anode and a cathode plate (both Bio-Rad Criterion anode plates with plastic housings modified to allow the electrodes to be brought into close proximity) were each attached to laser-cut plastic alignment casings (Figure S5A).[29] The electrode plates were separated by 3 mm shims placed on either side of the electrode surface and magnetically brought into contact (Figure S5B). The semi-dry electrotransfer system was connected to a power supply (Bio-Rad PowerPac Basic).

Probe electrophoretic mobility characterization

To characterize the probe μ_{gel} in a sizing gel, the electromigration of a discrete probe band using the slab-gel electrotransfer system was monitored. The semi-dry electrotransfer system was first used to electrophoretically inject probe from a free-solution layer between a sizing gel and a 20%T PA gel into the sizing gel (Figure S5D-F). The semi-dry electrotransfer system was connected to a power supply. The power supply was set to constant voltage and an electric field of 100 V/cm was applied for 30 s. After the power supply was turned off, the semi-dry electrotransfer system was dissasembled and the sizing gel was retrieved. A filter paper – sizing gel – filter paper sandwich was then assembled, and the sandwich was transferred into the acrylic clamp as described in subsection *Gel sandwich assembly for electrotransfer probing*. Finally, the clamped gel sandwich was inserted to the slab-gel electrotransfer system and probe x_E was monitored (sizing gel microwell-patterned face aimed towards the cathode; electric field = 12 V/cm, applied time = 30s, 60s, 120s, 180s, 240s, 300s). Probe electromigration distance was recorded for each electrotransfer time, and a least-squares linear-regresion fit was applied to determine the in-gel probe electrophoretic mobility.

Gel sandwich assembly for diffusive transfer probing

To load probe by diffusive transfer to a sizing gel, a gel sandwich was made using two loading gels and a sizing gel. First, a sizing gel was trimmed to final x-y-z dimensions: 5-5-1 mm. The loading gels were then trimmed to final x-y-z dimensions: 7-7-1 mm. Then, a sizing gel was placed on top of a loading gel (gel x-y faces in contact). Next, a second loading gel was placed on top of the sizing gel. The three-gel sandwich was then stored in a dark, humid chamber (single well of a 96-well plate) at 4 °C. No air bubbles were trapped between the gel layers during sandwich assembly. To unload probe by diffusive transfer, a probe loaded gel was placed in a single well of a 96-well plate. The well was filled with Electrotransfer Buffer (~300 µL), and buffer was refreshed every 6 h. The 96-well plate was stored in the dark at 4 °C. Times of diffusive probe transfer are described in Table S5.

OVA in-gel immobilization and probing

A solution of ovalbumin labelled with AlexaFluor® 488 (OVA, diluted to 5 µM in 1X Tris-glycine; No. 034783, Thermo Fisher Scientific) was electrophoretically injected into a sizing gel and immobilized in-gel. To electrophoretically inject OVA, the custom semi-dry electrotransfer system was used (system and sample assembly described in the subsection *Probe electrophoretic mobility characterization*). All gels were equilibrated in 1X RIPA buffer (instead of Electrotransfer Buffer; Table S2) immediately after fabrication at 4 °C for at least 12 h and up to 4 days prior to use. The filter paper was also equilibrated in 1XRIPA buffer (instead of Electrotransfer Buffer). After assembling the semi-dry electrotransfer system, a 35 mA constant current was applied for 15 s. Once the power supply was turned off, the system was disassembled and the sizing gel was exposed to UV light for 45 s to photocapture OVA to the BPMA-functionalized sizing gel as previously described.[27] Next, the sizing gel was incubated in Electrotransfer Buffer at 4 °C for at least 12 h to exchange buffers and unload unbound OVA (dark, 4 °C). In-gel immobilized OVA was probed by electrotransfer and diffusive transfer using 1° and 2° Ab probes (probes described in Table S3; probe transfer conditions described in Tables S4 and S5). Between each probe loading and unloading step, the sizing gel was incubated in a humid chamber for equilibrium immunocomplex formation (dark, ~20 °C). Incubation times for electrotransfer probing were informed by existing hydrogel immunoassay devices (1 °Ab incubation: 2 h; 2 °Ab incubation: 1 h).[3] In summary, the full 1° and 2° Ab probing sequence included: (i) 1°Ab probe loading, (ii) OVA-1°Ab probe equilibrium immunocomplex formation (2 h), (iii) 1°Ab probe unloading, (iv) 2°Ab probe loading, (v) 1°Ab-2°Ab probe equilibrium immunocomplex formation (1 h), and (vi) 2°Ab probe unloading.

Imaging and analysis

Image capture was performed with MetaMorph® imaging software (Molecular Devices) using an Olympus IX51 inverted widefield fluorescence microscope fitted with an Olympus UPlanFLN 4X objective (No. UPLFLN4X) and an X-Cite® illumination source (Excelitas Technologies), CoolSNAP™ HQ2 CCD camera (Teledyne Photometrics), GFP filter set (Chroma 49011 ET), DAPI filter set (Chroma 4900), and TRITC filter set (Chroma 41002c).

Image acquisition of in-gel fluorescence resulting from probe loading and unloading was performed by placing the sizing gel on a 65mm Petri dish (10-10 mm gel x-y face in contact with the Petri dish). The microscope plane of focus was adjusted to the middle-depth of the 1 mm sizing gel. Average in-gel fluorescence was calculated. Background subtraction was performed by subtracting the average in-gel fluorescence of gels with no exposure to fluorescent probe molecules from the average in-gel fluorescence of test group gels. Effective partition coefficients were calculated as the ratio of the average in-gel fluorescence of the sizing gel after loading over the average in-gel fluorescence of the loading gel after fabrication (effective partition coefficient determined following this calculation for both electrotransfer and diffusive probe loading). For probe loading by diffusive transfer, a Power

Law[30,31] model for total probe mass loading was fit to in-gel fluorescence timepoint measurements using MATLAB®. In MATLAB, the fit() function and a custom-defined equation to model Power Law probe loading was used (Figure 4B)

$$Fluorescence\ in\ gel = \frac{[Ab]_t}{[Ab]_\infty} = a * t^b \quad (3)$$

where $[Ab]_t$ is probe mass in gel at time t, $[Ab]_\infty$ is the probe mass in gel at equilibrium, a is a structural constant of the gel, and b is a release exponent.[30,31] Model fit paramters were: a = 104.1, b = 0.1992, r^2 = 0.9321‡.

To calculate probe unloading, the average in-gel fluorescence after unloading was normalized to the average in-gel fluorescence after loading. For probe unloading by diffusive transfer, a Power Law[30,31] model was fit to in-gel fluorescence timepoint measurements using MATLAB®. In MATLAB, the fit() function and a custom-defined equation to model Power Law probe unloading was used (Figure 5B)

$$Fluorescence = \frac{[Ab]_t}{[Ab]_\infty} = 1 - a * t^b \quad (4)$$

where $[Ab]_t$ is probe mass in gel at time t, $[Ab]_\infty$ is the probe mass in gel at equilibrium, a is a structural constant of the gel, and b is a release exponent.[30,31] Model fit paramters were: a = 0.1766, b = 0.4236, r^2 = 0.9812.

To image probe peak location in the probe electrophoretic mobility characterization, and the immobilized OVA and probed signal peak locations in the OVA immunoprobing experiments, a razor was used to cut a 0.5 mm sliver of the sizing gel (10mm x ~0.5mm x 1mm in x-y-z; Figure S6A). The sizing gel sliver was laid on a 65 mm Petri dish (10 mm x 1 mm sliver x-z face in contact with the Petri dish (Figure S6B). Fluorescence profiles in the z-axis were computed by averaging fluorescence intensities across ~2 mm image region in the x-axis at each z-axis depth (Figure S6B for axis orientation). Averaged fluorescence profiles were fit with Gaussian curves to determine peak location (MATLAB®, fit() function, 'gauss1' fit model, region analysed: peak location ± 3σ). Background subtraction performed by subtracting the average pixel value in the 3σ to 4σ region (defined as background) from the pixel values in the peak location ± 3σ region (defined as signal). Background noise for determining SNR values of probed signal was calculated by taking the standard deviation of the fluorescence intensity between the 3σ and 4σ bounds of the fluorescence profiles. Peak location was determined by the peak location of the Gaussian fit.

Results and discussion

Electrolytic cell design for electrotransfer probing

To improve the in-gel immunoassay detection sensitivity determined by diffusive probe transfer, we sought to address the following immunoprobing design criteria: (i) near complete probe loading (K_{part}~1) and unloading in a hydrogel, and (ii) rapid probe loading and unloading in a hydrogel compared to immunocomplex dissociation timescales. PA protein sizing gels designed with 10-100 nm average pore radii are used to resolve proteins with molecular weights of ~10-90 kDa,[32] corresponding to hydrodynamic radii (R_h) of ~1.5-4.0 nm.[33] Size-exclusion partitioning of diffusively loaded probe to hydrogels reduces the equilibrium K_{part} of the probe, and can be approximated using Ogston's model[10,11]

$$K_{part} = \frac{[Ab]_{gel}}{[Ab]_{sol}} = \exp\left(-\phi\left(1 + \frac{R_h}{a_f}\right)^2\right) \quad (5)$$

where ϕ is the volume fraction of polymer in the gel, and a_f (nm) is the polymer fiber radius of the gel. The average pore size of a gel is related to ϕ through a negative exponential relationship.[34] Thus, increasing ϕ causes exponential decreases in average gel pore size and K_{part}. For gel fabrication, ϕ is linearly related to total acrylamide monomer density ($\%T$), and gel $\%T$ can be tuned to control gel pore size (for fixed percent bis-acrylamide cross-linker, $\%C$). When using large antibody probes (150 kDa, R_h~5 nm)[13] to diffusively probe protein sizing hydrogel (7-12%T, 2-5%C), $[Ab]_{gel}$ can be an order of magnitude lower than $[Ab]_{sol}$ (Figure 1F).[3,6,7,35]

Long diffusive probe unloading timescales compared to immunocomplex dissociation reduces the concentration of immunocomplex remaining at time of assay readout.[36] The expected 1-dimensional probe diffusion distance, $\langle x_{Diff} \rangle$ (μm), is linearly related to the square-root of time given by[34,37]

$$\langle x_{Diff} \rangle = \sqrt{2 D_{\%T} t} \quad (6)$$

$$D_{\%T} = D_{sol} \exp\left(-3.03\ {R_h}^{0.59}\ \%T^{0.94}\right) \quad (7)$$

where $D_{\%T}$ (μm²·s⁻¹) is the in-gel diffusion coefficient of the probe, D_{sol} is the free-solution diffusion coefficient of the probe. An analytical model shows that in the time required for antibody diffusion across 1.2 mm of a 7%T, 2.7%C PA gel to occur (~53 h), <50% of initial immunocomplex will remain intact for antibodies with k_{off} > 10^{-6} s^{-1} (Figure 1G).

In contrast to diffusive probe migration, probe electromigration velocity (v; μm·s⁻¹) is linearly proportional to strength of applied electric field (E; V·cm⁻¹)

$$v = \mu_{gel} E \quad (8)$$

$$\mu_{gel} = \frac{q}{6\pi\eta R_h} 10^{-K_r \%T} \quad (9)$$

where q (C) is the molecule net charge, η (Pa·s⁻¹) is the solution viscosity, K_r is the gel retardation coefficient, and μ_{gel} (cm²·V⁻¹·s⁻¹) is the in-gel electrophoretic mobility of the probe. E thus provides a tuneable parameter to expedite probe electromigration and increase K_{part} (compared to diffusive probing) without altering gel pore size.[38] Additionally, the probe electromigration distance (x_E; μm) is linearly related to t, whereas $\langle x_{Diff} \rangle$ is linearly related to the square-root of t (x_E~t; $\langle x_{Diff} \rangle$~$\sqrt{t}$).[39]

$$x_E = \mu_{gel} E t \quad (10)$$

We thus designed an electrotransfer probing platform to satisfy the design criteria of increased K_{part} and expedited probe transfer compared to diffusive probing. In electrotransfer probing: (i) probe

is loaded to a small pore sizing gel (7%T, 3.5%C PA gel, pore radius ~40-87 nm[40]) by electrotransfer from an inert, large pore probe loading gel (1.5% w/v agarose, pore radius ~100-150 nm[41]), (ii) probe is incubated in the sizing gel to reach immunocomplex equilibrium, and (iii) probe is unloaded by electrotransfer from the sizing gel (Figure 2A-C). Our system involves sandwiching the loading gel and sizing gel together, and performing probe electrotransfer in an electrolytic cell using a conventional slab-gel electrotransfer system to supply uniform electric field across the gel. We designed an inert, large pore loading gel to facilitate electrotransfer of nearly all antibody probe mass from the loading gel to the sizing gel. We evaluated timescales of electrotransfer probe loading and unloading, and mass of probe loaded and unloaded in a sizing gel. Finally, we investigated the impact of electrotransfer probing on the detection sensitivity of a protein sizing in-gel immunoassay in a proof-of-concept demonstration by immunoprobing for in-gel immobilized OVA.

Electrotransfer probing design mitigates the negative impacts of electrolysis products on electromigration performance

To predict probe loading and unloading in a hydrogel by electrotransfer without direct visualization of probe location, the relationship between x_E, E, and t given by Equation 10 can be used as long as key parameters such as q and E remain constant. In designing the electrogransfer probing system, we considered that unpredictable or poorly reproducible in-gel electromigration within an electrolytic cell (not adhering to Equation 10) can result from the gas and ionic products of the electrolysis reactions occuring at the electrode surfaces:[42]

$$Cathode: 2H_2O_{(l)} + 2e^- \leftrightarrow 2OH^-{}_{(aq)} + H_{2(g)} \quad (11)$$

$$Anode: H_2O_{(l)} \leftrightarrow 2e^- + 2H^+{}_{(aq)} + \frac{1}{2}O_{2(g)} \quad (12)$$

Specifically, the gas bubble products of electrolysis can obstruct the electric field path, and cause time-variable voltage drops (and thus E) across gels.[43] To remove electrolysis gas bubbles from the path of the applied E, a conventional slab-gel electrotransfer chamber was custom-fit with an acrylic gel clamp (Figure SI1). The clamp facilitated bubble removal from the E path by including an open buffer solution – air interface, permitting bubbles to float to the surface of the buffer volume as they are generated.

Deviations from theoretical electromigration behavior (Equation 10) can also result from the strong base (OH-) and strong acid (H+) products of electrolysis. The strong base and acid products can cause sharp pH changes near the electrode surfaces, specifically making the solution near the cathode more basic and the solution near the anode more acidic.[42,44] This phenomenon has been well reported in similar systems, particularly for capillary electrophoresis[42] and has even been applied to form natural pH gradients in isoelectric focusing systems.[44] Such pH variation can cause changes in μ_{gel} by altering the probe q (Equation 9).[45]

A previously established modelling framework[42] predicted pH in buffer solution as a result of applied E and t (total charge delivered). Briefly, total charge delivered from electrodes to solution was calculated using Faraday's law of electrolysis from applied electric current intensity and duration. The total charge delivered was used to calculate the change in [H+] or [OH-] (from surface of anode or cathode, respectively) in solution, and the ion concentration change was used along with initial buffer ion concentrations and buffer pKa to calculate system pH. System pH was then reported as a function of the distance from each electrode surface (where the total number of buffering species available to mitigate pH change is a function of increasing buffer volume). The results of this modeling analysis are included in Figure 2D, which shows the expected pH as a function of distance from each electrode surface in this system. For a 1X-Tris-glycine buffer volume with dimensions 10 cm x 10 cm x 2.5 cm (width x height x depth, 250cm^3 total volume) the center 1 mm between the electrodes (distance between opposite faces of the sizing gel) experiences minimal pH changes (0.031 difference in pH, within the variability of 1X Tris-glycine made from commercially available stock solution[46] and below the resolvable pI difference demonstrated in single-cell isoelectric focusing technologies[47]). Thus, we designed a system in which gas products of electrolysis could be passively removed and ionic products would cause negligible pH changes (as suggested by modeling analysis).

Probe electromigration distance is linearly dependent on time in electrotransfer system

We next sought to experimentally demonstrate that probe x_E responds linearly with t, and calculate the probe μ_{gel} in our system. To monitor probe x_E, probe was electrophoretically injected into the gel from free-solution using a custom made semi-dry electrotransfer system (Figure S5). The probe sample underwent electrophoretic sample stacking (lower probe μ_{gel} than probe free-solution electrophoretic mobility, Equation 9). Because the probe solution initially formed a thin layer and underwent sample stacking, the width of the probe band in-gel (Gaussian fit, ± 3σ) was less than the gel thickness. The location of the migrating probe band was tracked by fitting a Gaussian curve to identify the probe peak location. The in-gel x_E of the probe band in the electrotransfer probing system was then charcterized over t.

A linear relationship between probe x_E and t in electromigration was determined using a least-squares linear-regression model (r^2 = 0.9888, Figure 2E). The probe v for the applied E was extracted from the slope of the linear fit (v = 2.17 μm/s) and the $\mu_{7\%T}$ for the probe in this system was determined using Equation 8; $\mu_{7\%T}$ = 1.81 x 10^{-5} cm^2/(V·s). No significant difference in x_E across gels was observed, facilitating prediction of probe location in-gel without real-time vizualization of probe location ($p > 0.22$, Mann-Whitney U-test; Figure 2E). As described by Equation 9, $\mu_{7\%T}$ can vary across molecular species in native electrotransfer conditions by r_h and q of a probe. However, in the case of antibody probes within the same antibody class (isotype), large variations in electrophoretic mobility are not expected, owing to minimal variation of r_h and q. Antibodies of the IgG isotype were used here and are predominantly used as primary and secondary probes in western blots and other immunoassays. Recharacterization of probe $\mu_{7\%T}$ would be required if antibodies of different classes were used, (e.g. IgM instead of IgG), as different isotypes can be expected to vary substantially in r_h and q. Additionally, probe conjugation with labels of varied charge may

impact q of the label conjugated probe and thus also require $\mu_{7\%T}$ recharacterization.

Electrotransfer yields near-complete probe release from an agarose loading gel

To maximize utility across a range of in-gel immunoassays, we designed the probe loading gel with two key traits: (i) rapid fabrication and assembly with minimal handling, and (ii) efficient probe release (minimal probe entrapment in loading gel) to maximize the amount of probe available for loading into the immunoassay gel. We hypothesized that an inert hydrogel with large pores (100-1000 nm pore radius) could be used as a probe loading gel to satisfy these two design criteria. We thus used a 1.5% low melting point agarose gel as a model probe loading gel (Figure S2).[48] To assess probe release efficiency, we then compared probe release from an agarose loading gel to probe release from a 4%T PA loading gel. Electrotransfer parameters were chosen for a calculated probe $\boldsymbol{x_E} >$ 1500 μm, whereas the loading gel thickness was 1000 μm (Equation 10; Figure 2E).

After unloading, the fluorescence remaining in the agarose loading gel was 3.93% ± 1.76% of the initial in-gel fluorescence (error reported as standard deviation, n=3, Figure 3). The fluorescence remaining in the 4%T PA loading gel was 75.8% ± 12.3% of the initial in-gel fluorescence (error reported as standard deviation, n=6, Figure 3). The agarose loading gel thus retained ~19X less probe than the PA loading gel after unloading by electrotransfer (p=0.0238, Mann-Whitney U-test).

Interestingly, the majority of the probe in the 4%T PA loading gel precursor solution remained in-gel after unloading by electrotransfer. From calculations of probe $\boldsymbol{x_E}$ for applied $\boldsymbol{E}$ and $\boldsymbol{t}$ (Equation 10), we expected probe to unload from the 4%T PA loading gel (calculated $\boldsymbol{x_E}$ > 1500 μm in a 7%T PA gel, and therefore also in a 4%T PA loading gel). We therefore do no attribute the observed signal to insufficient applied $\boldsymbol{E}$ or $\boldsymbol{t}$. However, the free radical cascade resulting from chemically initiated (APS & TEMED) PA gel polymerization is known to interact with proteins that are included in PA gel precursor solutions. This interaction has been shown to cause protein denaturation in PA gels during polymerization, evidenced by western blotting analysis.[49] Additionally, incomplete macromolecule drug release from hydrogel drug-delivery devices has been observed for hydrogel devices that were polymerized with drug included in the gel precursor solution.[31,50] Probe remaining in the 4%T PA gel after electrotransfer unloading may thus be caused by similar interactions, causing denatured probe to be entropically trapped in the pores or immobilization of the probe to the hydrogel matrix.[50] Agarose gelation does not undergo the same polymerization process and is relatively inert to proteins while transitioning from molten to solidified states[51]. The inert nature of the large-pore agarose loading gel satisfies the design criteria of both minimal probe entrapment in-gel and rapid, straightforward fabrication.

Probe is rapidly loaded with enhanced partition coefficient in electrotransfer probing

After designing a system for controllable constant-velocity probe electromigration (r^2 = 0.9888, Figure 2E) and minimal probe entrapment in an agarose loading gel (96.07% ± 1.76% probe removed, Figure 3A), we aimed to demonstrate this system for an increased K_{part} and rapid probe transfer from the loading gel to a sizing gel in electrotransfer probe loading (as compared to diffusive probing; design criteria of diffusive probing system were informed by previous work[52] and are described in Note S1). To determine the expected probe x_E in the system for an applied E, the probe $\mu_{7\%T}$ calculated from Figure 2E was again used. At $E =$ 8 V/cm, expected $v =$ 1.45 μm/s, and the calculated t required for probe to electromigrate 1000 μm (sizing gel thickness) was ~11.5 min. Probe μ_{gel} in the 1.5% agarose loading gel is expected to be greater than in the 7%T PA sizing gel based on previous comparisons of electrophoretic macromolecule transport in the two materials (larger pore size in agarose gel permits faster macromolecule transport).[48] Because of this difference in μ_{gel} values, it is expected that probe electrotransferring from the loading gel to the sizing gel will undergo electrophoretic stacking, becoming more concentrated upon entering the sizing gel by the ratio of the two μ_{gel} values.[53] As the loading gel and the sizing gel are the same thicknesses (1 mm), we hypothesized this electrophoretic stacking to minimize the extent of probe loss from gel to the surrounding buffer solution by diffusive broadening during probe electromigration. The mean effective K_{part} for electrotransfer probe loading was $K_{part,E}$ = 0.87 ± 0.05 (n=4, error reported as standard deviation; Figure 4A).

The duration for monitoring diffusive probe loading was informed by Equations 6 and 7. Probe diffusion over 0.5 mm in a 7%T PA gel (minimum characteristic diffusion length, as probe is loaded from both opposite faces of the 1mm thick sizing gel) is expected to occur in ~4.8 h (τ). In-gel fluorescence measurements were recorded over 28 h (>5.8 τ) of diffusive probe loading. The mean K_{part} after 28 h of diffusive transfer probe loading was $K_{part,diff}$ = 0.13 ± 0.01 (n=4, error reported as standard deviation; Figure 4A). Thus, mean effective K_{part} into the sizing gel was enhanced in electrotransfer probe loading compared to diffusive transfer probe loading by a factor of 6.5 ± 0.1 (p=0.0286, Mann-Whitney U-test).

To characterize probe loading over $\boldsymbol{t}$ by diffusive transfer, in-gel fluorescence over 28 h of diffusive probe loading was used to generate a Power Law model fit[30,31] (r^2 = 0.9321‡; Figure 4B). From the Power Law fit, 90% of in-gel fluorescence measured at 28 h was determined to occur at ~16 h. Electrotransfer probe loading thus not only resulted in an effective probe $\boldsymbol{K_{part}}$ that was 6.5 ± 0.1 X greater than in diffusive transfer loading, but was also demonstrated to do so >82X faster than diffusive transfer loading (electrotransfer loading time = 11.5 min).

Electrotransfer facilitates rapid, effective probe unloading

We next considered the probe fluorescence retained in the sizing gel after unloading by probe electrotransfer compared to diffusive transfer. To accomplish this, probe-loaded sizing gels were unloaded by either probe electrotransfer or probe diffusive transfer. The E and t (12 V/cm, 15 min) for removal of unbound probe was determined

from $\mu_{7\%T}$ calculated in Figure 2E. Calculations estimated probe $x_E \approx$ 2000 µm, thus supporting complete unloading of the sizing gel (1000 µm). After probe unloading by electrotransfer, the fluorescence retained in the sizing gel was 5.54% ± 1.16% (n=5, Figure 5A) of the initial probe-loaded sizing gel fluorescence. Probe unloading by diffusive transfer was expected to occur in ~4.8 h (τ; Figure 1C). After 45 h of diffusive washout (>9.7τ), we observed a mean in-gel fluorescence of 15.09% ± 4.62% (n=6, Figure 5A) of the initial in-gel probe-loaded sizing gel.

Interestingly, in-gel fluorescence during probe unloading by diffusive transfer continued to decrease over 45 h (n=3, Figure 5B). In order to characterize probe unloading over t by diffusive transfer, the in-gel fluorescence data during probe removal were fit to a Power Law[30,31] model of diffusive probe unloading (r^2 = 0.9812; Figure 5B). From the Power Law fit, 90% of unbound probe was removed at ~45 h. The rate of probe removal could be potentially expedited by more regular buffer bath exchanges (e.g., twice hourly, as is done for similar antibody probe removal steps from similarly dense PA gel immunoassays[3] instead of every 12 h as was done here), or storage in warmer environment (>4 °C). Such measures were not taken in these experimental procedures as 30 min buffer exchanges over >24 hour was not deemed experimentally practical, and to prevent sample contamination or antibody denaturation by additional handling steps and storage in warm environment. Ultimately, the remaining in-gel background fluorescence resulting from probe unloading by electrotransfer was 2.7 ± 0.4 X less than probe unloading by diffusive transfer and was accomplished >180X more rapidly than unloading by diffusive transfer.

Electrotransfer probing improves immunoassay performance compared to diffusive probing

Finally, we assessed the impact of electrotransfer probing on in-gel immunoassay detection sensitivity in comparison to diffusive transfer probing. We hypothesized that applying electrotransfer probing to detect OVA immobilized in a protein sizing gel would result in greater SNR and require less immunoprobing time than OVA detection by diffusive transfer probing. Fluorescence micrographs of the OVA and probe bands are shown in Figure 6A. We observed that the mean SNR in electrotransfer probing was 20.56 ± 15.60 (n=6), while that of diffusive transfer probing was 5.02 ± 1.70 (n=4, p=0.0095, Mann-Whitney U-test, Figure 6B). The SNR variability of electrotransfer probing may have been inflated by variable probe concentration in loading gels, as described in Table S3 (1° Ab probe: 0.1-0.0075 mg/mL, 2° Ab probe: 0.2-0.015 mg/mL). Loading gels used in diffusive probing did not vary in probe concentration (1° Ab probe: 0.1 mg/mL, 2° Ab probe: 0.2 mg/mL). Further experiments are required to investigate the effect of probe concentration in loading gels on SNR. An assessment of target protein peak location and detected probe peak location in electrotransfer and diffusive probing was performed to verify that the measured probe signal corresponded to the actual target protein location (p > 0.17 for both methods, Mann-Whitney U-test, Figure 6C). Notably, the total time required for completion of assay probing steps in electrotransfer and diffusive transfer probing differ greatly: the diffusive transfer probing was completed in 120 h while electrotransfer probing was completed in less than 4 h (Figure 6D). Compared to diffusive transfer probing, electrotransfer probing thus improved in-gel immunoassay detection sensitivity, marked by 4.1 ± 3.4 X greater SNR, and required 30X less immunoprobing time.

Conclusions

We introduced a gel-gel electrotransfer probing system for rapid and effective probe loading and unloading in mm-scale, dense, open in-gel immunoassays. Our design involves (i) an electrolytic cell that has been designed and characterized for predictable probe migration, and (ii) an agarose loading gel for low-loss delivery of probe to a protein-sizing gel. We demonstrated this system for faster, more effective probe loading and unloading to a large, dense, open hydrogel than possible with conventional diffusive transfer probing. We additionally evaluated the impact of electrotransfer probing on in-gel immunoassay detection sensitivity, using OVA detection from a protein sizing gel as a proof-of-concept example. Compared to diffusive transfer probing, we observed increased probed signal SNR in a substantially shorter overall immunoprobing duration. Electrotransfer probing both increased probed protein measurement SNR and required 30X less immunoprobing time than diffusive transfer probing. Given the prevalent usage of in-gel immunoassays for target protein detection from biological samples, we anticipate that electrotransfer probing will improve detection sensitivity across a wide range of in-gel immunoassays. Open questions include investigations of electrotransfer probing using alternative probe labels (e.g., fluorescent labels with varied charge). Additionally, by removing challenges to immunoprobing mm-scale protein sizing hydrogels, we anticipate electrotransfer probing to facilitate the design of novel in-gel immunoassays with expanded form-factors and enhanced precision protein characterization capabilities.

Conflicts of interest

The authors declare no competing financial interests.

Acknowledgements

This work was supported by the National Cancer Institute of the National Institutes of Health, Cancer Moonshot award (R33CA225296, to A.E.H.). S.M.G. was supported by a postdoctoral fellowship from the Natural Sciences and Engineering Research Council of Canada (NSERC). A.P.M was supported by National Institutes of Health training grant (T32GM008155) and a National Science Foundation Graduate Research Fellowship (1106400). Photolithography was performed in the QB3 Biomolecular Nanotechnology Center. The authors are grateful for discussions with all members of the Herr Lab.

Notes and references

‡ Goodness-of-fit for this model was evaluated by r-squared. Two outliers for this dataset were identified and were omitted from the data included in the model fit (1 at timepoint 10 h and 1 at timepoint 12.5 h). Measured fluorescence in the identified outliers was higher than expected because one face on the sizing gel was stippled with a microwell array (32 µm diameter, 40 µm depth, 100 µm center-to-center spacing), and this face was unintentionally faced upwards during imaging of in-sizing gel fluorescence. Fluorescently labelled

antibody solution was therefore able to pool in the microwells, artificially inflating measured antibody probe fluorescence in the sizing gel for the two outlier measurements. All other fluorescence measurements (across all gels and timepoints) were taken with microwells facing down. Including the outliers, the model fit paramters using the same Power Law process are: a = 108.9, b = 0.2046, r^2 = 0.7886.

1 J. Berg, T. JL and S. L., in *Biochemistry*, 5th ed.

2 C. Vogel, R. D. S. Abreu, D. Ko, S. Le, B. A. Shapiro, S. C. Burns, D. Sandhu, D. R. Boutz, E. M. Marcotte and L. O. Penalva, *Mol. Syst. Biol.*, 2010, **6**, 1–9.

3 A. J. Hughes, D. P. Spelke, Z. Xu, C.-C. Kang, D. V Schaffer and A. E. Herr, *Nat. Methods*, 2014, **11**, 455–464.

4 F. Chen, P. W. Tillberg and E. S. Boyden, *Science (80-.).*, 2015, **347**, 543–548.

5 I. Costantini, J. P. Ghobril, A. P. Di Giovanna, A. L. Allegra Mascaro, L. Silvestri, M. C. Müllenbroich, L. Onofri, V. Conti, F. Vanzi, L. Sacconi, R. Guerrini, H. Markram, G. Iannello and F. S. Pavone, *Sci. Rep.*, 2015, **5**, 9808.

6 M. J. Theisen, M. L. Chu and A. Laboratories, *In-gel Immunochemical Detection of Proteins that Transfer Poorly to Membranes*, 2004.

7 S. Desai, B. Dworecki and E. Cichon, *Anal. Biochem.*, 2001, **297**, 94–98.

8 J. Vlassakis and A. E. Herr, *Anal Chem*, 2015, **87**, 11030–11038.

9 J. A. Goodrich and J. F. Kugel, *Binding and Kinetics for Molecular Biologists*, Cold Spring Harbor Laboratories Press, Cold Spring Harbor, 2007.

10 A. G. Ogston, *Trans. Faraday Soc.*, 1958, **54**, 1754–1757.

11 J. Tong and J. L. Anderson, *Biophys. J.*, 1996, **70**, 1505–1513.

12 A. Su, B. E. Smith and A. E. Herr, *Anal Chem*, 2020, 875–883.

13 T. Jøssang, J. Feder and E. Rosenqvist, *J. Protein Chem.*, 1988, **7**, 165–171.

14 D. J. MacPhee, *J. Pharmacol. Toxicol. Methods*, 2010, **61**, 171–177.

15 W. N. Burnette, *Anal. Biochem.*, 1981, **112**, 195–203.

16 H. Towbin, T. Staehelin and J. Gordon, *Proc. Natl. Acad. Sci.*, 1979, **76**, 4350–4354.

17 G. J. Anderson, C. M. Cipolla and R. T. Kennedy, *Anal. Chem*, 2011, **83**, 17.

18 S. Jin, M. D. Furtaw, H. Chen, D. T. Lamb, S. A. Ferguson, N. E. Arvin, M. Dawod and R. T. Kennedy, *Anal. Chem.*, 2016, **88**, 6703–10.

19 C. Kotsmar, T. Sells, N. Taylor, D. E. Liu, J. M. Prausnitz and C. J. Radke, *Macromolecules*, 2012, **45**, 9177–9187.

20 S. H. Gehrke, L. H. Uhden and J. F. McBride, *J. Control. Release*, 1998, **55**, 21–33.

21 R. E. Gerver and A. E. Herr, *Anal. Chem.*, 2014, **86**, 10625–10632.

22 S. N. Krylov, *Electrophoresis*, 2007, **28**, 69–88.

23 J. Berthier, K. A. Brakke and E. Berthier, *Open Microfluidics*, Wiley, 2016.

24 T. Pfohl, F. Mugele, R. Seemann and S. Herminghaus, *ChemPhysChem*, 2003, **4**, 1291–1298.

25 G. V. Kaigala, R. D. Lovchik and E. Delamarche, *Angew. Chemie Int. Ed.*, 2012, **51**, 11224–11240.

26 C.-C. C. Kang, K. A. Yamauchi, J. Vlassakis, E. Sinkala, T. A. Duncombe and A. E. Herr, *Nat Protoc*, 2016, **11**, 1508–1530.

27 G. Dormán, H. Nakamura, A. Pulsipher and G. D. Prestwich, *Chem. Rev.*, 2016, **116**, 15284–15398.

28 A. W. P. Vermeer and W. Norde, *Biophys. J.*, 2000, **78**, 394–404.

29 S. M. Grist, A. P. Mourdoukoutas and A. E. Herr, *bioRxiv*, 2019, doi: https://doi.org/10.1101/805770.

30 J. Siepmann and N. A. Peppas, *Adv. Drug Deliv. Rev.*, 2001, **48**, 139–157.

31 C. C. Lin and A. T. Metters, *Adv. Drug Deliv. Rev.*, 2006, **58**, 1379–1408.

32 A. L. Shapiro, E. Viñuela and J. V. Maizel Jr., *Biochem. Biophys. Res. Commun.*, 1967, **28**, 815–820.

33 H. P. Erickson, *Biol. Proced. Online*, 2009, **11**, 32–51.

34 H. Park, C. S. Johnson and D. A. Gabriel ', *Macromolecules*, 1990, **23**, 1548–1553.

35 K. A. Yamauchi and A. E. Herr, *Microsystems Nanoeng.*, 2017, **3**, 16079.

36 S. J. Shapiro, D. Dendukuri and P. S. Doyle, *Anal. Chem.*, 2018, **90**, 13572–13579.

37 H. Berg, *Random walks in biology*, 1993.

38 K. Ferguson, *Metab., Clin. Exp*, 1964, **13**, 985–1002.

39 T. M. Squires, R. J. Messinger and S. R. Manalis, *Nat. Biotechnol.*, 2008, **26**, 417–426.

40 D. L. Holmes and N. C. Stellwagen, *Electrophoresis*, 1991, **12**, 612–619.

41 J. Narayanan, J.-Y. Xiong and X.-Y. Liu, *J. Phys. Conf. Ser.*, 2006, **28**, 83–86.

42 H. Corstjens, H. A. H. Billiet, J. Frank and K. C. A. M. Luyben, *Electrophoresis*, 1996, **17**, 137–143.

43 C. W. M. P. Sillen, E. Barendrecht, L. J. J. Janssen and S. J. D. van Stralen, *Int. J. Hydrogen Energy*, 1982, **7**, 577–587.

44 K. Macounová, C. R. Cabrera, M. R. Holl and P. Yager, *Anal Chem*, 2000, **72**, 3745–3751.

45 B. Bjellqvist, K. Ek, P. Giorgio Righetti, E. Gianazza, A. Görg, R. Westermeier and W. Postel, *J. Biochem. Biophys. Methods*, 1982, **6**, 317–339.

46 A. M. Tentori, K. A. Yamauchi and A. E. Herr, *Angew Chem Int Ed Engl*, 2016, **55**, 12431–12435.

47 Tris-Glycine Buffer (TG Buffer), pH 8.3±0.2, 10X Concentrate, https://www.polysciences.com/default/catalog-products/life-sciences/buffers/tris-glycine-buffer-tg-buffer-ph-8-3-0-2-10x-concentrate/, (accessed 26 January 2020).

48 N. C. Stellwagen, *Electrophoresis*, 2009, **30(Supp1)**, S188-95.

49 J. M. Brewer, *Science (80-.).*, 1967, **156**, 256–257.

50 C. C. Lin and A. T. Metters, *Pharm. Res.*, 2006, **23**, 614–622.

51 S. Magdelin, *Gel Electrophoresis - Principles and Basics*, Rijeka, Croatia, 2012.

52 A. Geldert, H. Huang and A. E. Herr, *Sci. Rep.*, 2020, **10**, 1–12.

53 J. M. Walker, in *Basic Protein and Peptide Protocols*, Humana Press, 2003, pp. 17–22.

Main Figures Only

Rapid electrotransfer probing for improved detection sensitivity in in-gel immunoassays

Analytical Methods: AY-ART-06-2020-001203.R1

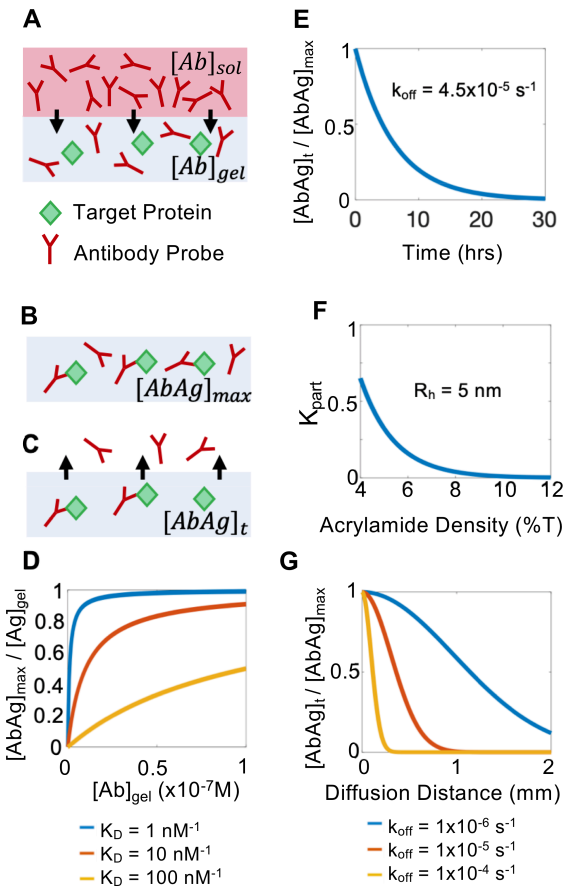

Figure 1. Immunocomplex remaining at time of assay readout is reduced by long probe diffusion distances and small pore-gel size ratio. (**A**) Probe loading into an immunoassay gel (shown in light blue). (**B**) In-gel probe incubation for equilibrium immunocomplex formation. (**C**) Unloading of unbound probe from the immunoassay gel. (**D**) Equilibrium immunocomplex formation, $[AbAg]_{max}$, is maximized by increasing concentration of antibody probe in-gel, $[Ab]_{gel}$. (**E**) Substantial immunocomplex dissociation occurs over hours-long timescales for medium dissociation rate constant, k_{off}. (**F**) Antibody probe partition coefficient, K_{part}, is reduced below 0.25 for polyacrylamide protein sizing gels (7-12%T, 2.7%C). (**G**) Substantial immunocomplex dissociation occurs over a range of k_{off} values during time required for diffusive probe unloading of millimeter scale protein sizing gels (7%T, 2.7%C).

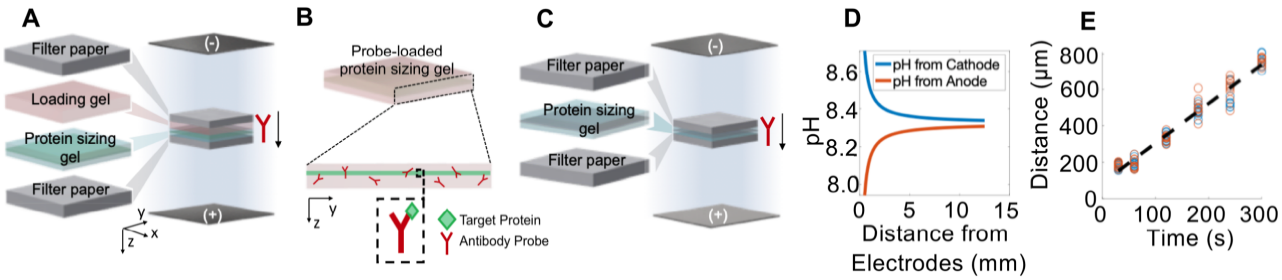

Figure 2. Electrotransfer probing facilitates predictable probe electromigration without direct visualization. (**A**) Probe Loading: A sandwich of filter papers, a loading gel, and a protein sizing gel is submerged in a buffer volume. Probe is loaded to the sizing gel by electrotransfer. (**B**) Equilibrium Immunocomplex Formation: The probe-loaded sizing gel is removed from buffer volume for equilibrium immunocomplex formation. (**C**) Probe Unloading: A sandwich of filter papers and the sizing gel is submerged in a buffer volume and unbound probe is unloaded from the sizing gel by electrotransfer. (**D**) pH stability at the center of electrolytic cell is predicted by modeling analysis of pH resulting from applied current to electrotransfer probing system. The gel sandwiches are located at the center of the 2.5 cm wide electrolytic cell (12.5 mm from each electrode). (**E**) Probe electromigration distance is linearly related to time ($r^2 = 0.9888$, least-squares linear-regression model). Five trials were performed at varied electromigration times (t = 30s, 60s, 120s, 180s, 240s, 300s) using two gels per trial (separate gels are colour-coded). No significant difference was observed across individual gels used in each trial ($p > 0.22$, Mann-Whitney U-test).

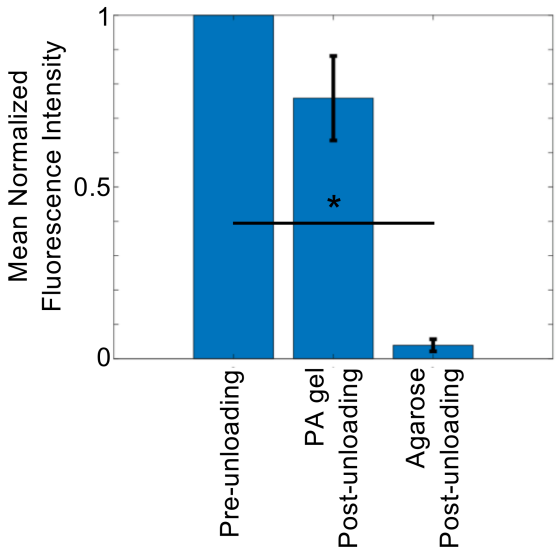

Figure 3. Unbound probe entrapment in loading gels after unloading by electrotransfer (12 V/cm, 12 minutes). Loading gels were fabricated with 0.2 mg/ml Donkey anti-Rabbit AF647 antibody included in molten (1.5% w/v agarose gel) or unpolymerized (4%T, 3.5%C PA gel) states. Pre-unloading: n=9. PA gel Post-unloading: n=6. Agarose Post-unloading: n=3. Error bars indicate standard deviation. (* *indicates statistical difference by Mann-Whitney U-test, p<0.0238*)

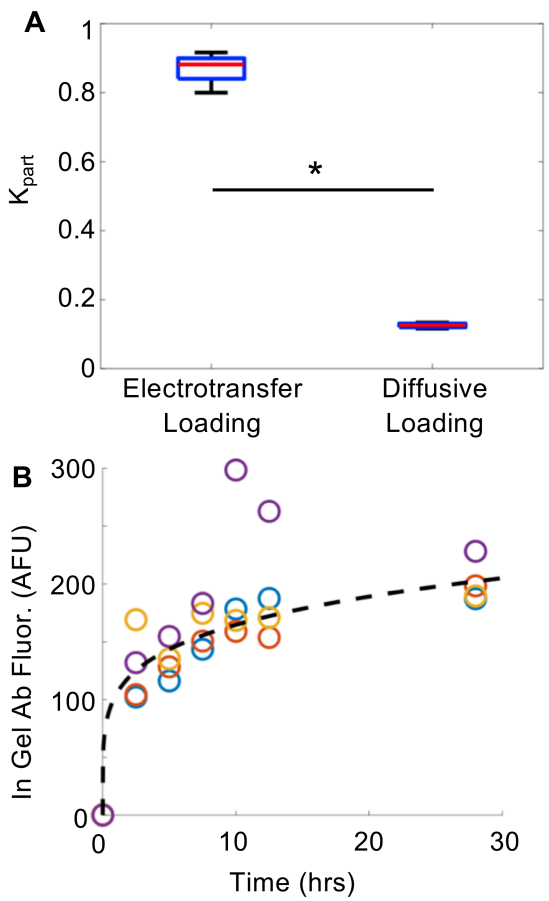

Figure 4. (**A**) Electrotransfer probe loading results in greater partition coefficient than diffusive probe loading. Electrotransfer loading n=4. Diffusive loading n=4. (** indicates statistical difference by Mann-Whitney U-test, p=0.0286*) (**B**) Diffusive probe loading to a sizing gel occurs over hours-long timescale (n=4, separate gels are color coated).

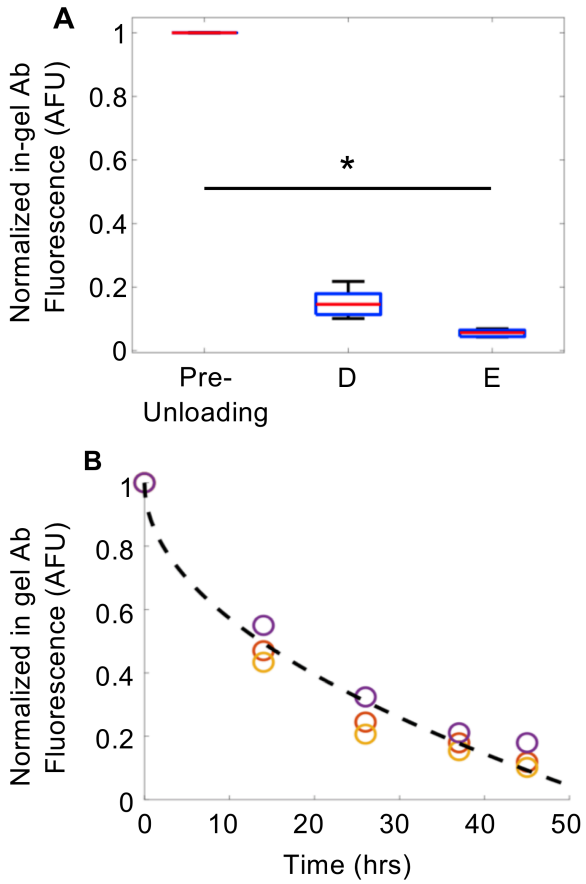

Figure 5. (**A**) Electrotransfer unloading of unbound probe results in less probe entrapment in-gel than diffusive unloading. E: electrotransfer unloading, n=5. D: diffusive unloading, n=6. (** indicates statistical difference by Mann-Whitney U-test, p<0.05*) (**B**) Diffusive probe unloading from a sizing gel occurs over hours-long timescale (n=3, separate gels are color coated).

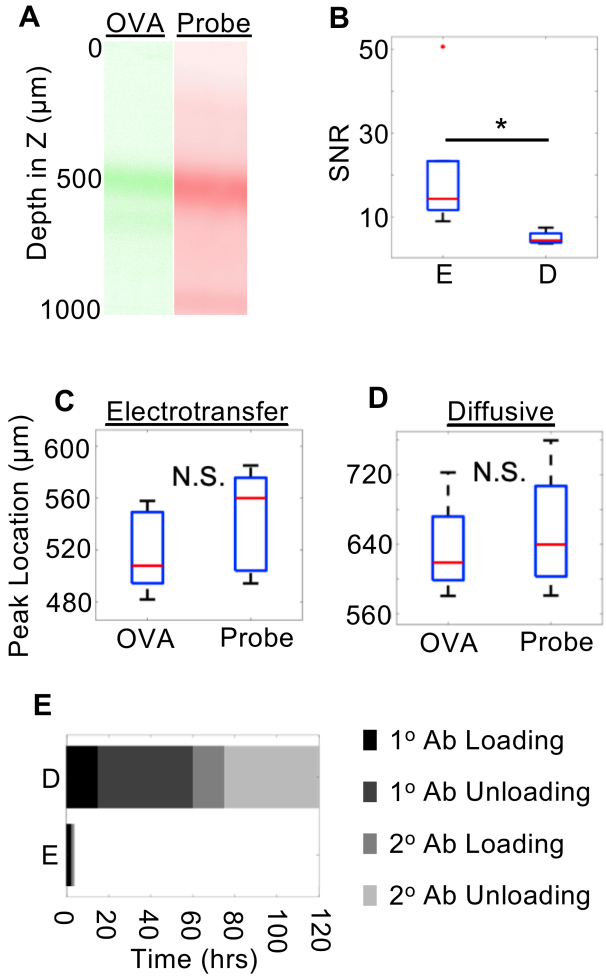

Figure 6. Electrotransfer probing detects in-gel immobilized OVA with greater SNR and less immunoprobing duration than diffusive probing. (**A**) Fluorescence micrographs of immobilized OVA and electrotransfer detection probe in a sizing gel. (**B**) SNR of OVA detection probe in electrotransfer probing is greater than in diffusive probing. Electrotransfer: n=6. Diffusive: n=4. *(* indicates statistical difference by Mann-Whitney U-test, p=0.0095).* (**C,D**) Peak locations of target OVA protein and detection probe show no statistical difference in electrotransfer probing (**C**) and diffusive probing (**D**) conditions (p>0.17, *Mann-Whitney U-test*). (**E**) Immunoprobing duration is 30x shorter in electrotransfer probing than diffusive probing. E: electrotransfer probing. D: diffusive probing.

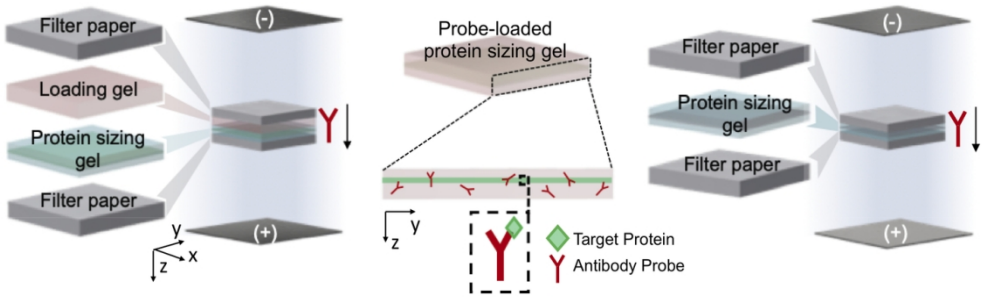

123x37mm (300 x 300 DPI)